Kinetics of Triscarbonato Uranyl Reduction by Aqueous Ferrous Iron: A Theoretical Study

Matthew C. F. Wander,*,† Sebastien Kerisit,‡ Kevin M. Rosso,‡ and Martin A. A. Schoonen†

Department of Geosciences and Center for Environmental and Molecular Science, Stony Brook University, Stony Brook, New York 11794-2100, and Pacific Northwest National Laboratory, Richland, Washington 99352

Received: April 14, 2006; In Final Form: June 5, 2006

Uranium is a pollutant whose mobility is strongly dependent on its oxidation state. While U(VI) in the form of the uranyl cation is readily reduced by a range of natural reductants, by contrast complexation of uranyl by carbonate greatly reduces its reduction potential and imposes increased electron transfer (ET) distances. Very little is known about the elementary processes involved in uranium reduction from U(VI) to U(V) to U(IV) in general. In this study, we examine the theoretical kinetics of ET from ferrous iron to triscarbonato uranyl in aqueous solution. A combination of molecular dynamics (MD) simulations and density functional theory (DFT) electronic structure calculations is employed to compute the parameters that enter into Marcus' ET model, including the thermodynamic driving forces, reorganization energies, and electronic coupling matrix elements. MD simulations predict that two ferrous iron atoms will bind in an inner-sphere fashion to the three-membered carbonate ring of triscarbonato uranyl, forming the charge-neutral ternary $Fe_2UO_2(CO_3)_3(H_2O)_8$ complex. Through a sequential proton-coupled electron-transfer mechanism (PCET), the first ET step converting U(VI) to U(V) is predicted by DFT to occur with an electronic barrier that corresponds to a rate on the order of $\sim 1\ s^{-1}$. The second ET step converting U(V) to U(IV) is predicted to be significantly endergonic. Therefore, U(V) is a stabilized end product in this ET system, in agreement with experiment.

Introduction

Uranium pollution, a consequence of uranium mining as well as nuclear research and development, is a problem that is complicated by many factors. Foremost of these is that uranium mobility is highly dependent upon its oxidation state. U(VI) is highly soluble and therefore mobile in oxic aqueous environments in the form of the divalent dioxouranium cation UO_2^{2+}. Electron transfer (ET) to U(VI) reduces it to less soluble forms, yielding the precipitation of insoluble uranium phases and effective immobilization.[1] Hence, many strategies are being developed to immobilize uranium by reduction. These include abiotic reactive barriers charged with reductants such as Fe(0), as well as the use of dissimilatory metal-reducing bacteria.[2−5]

Another factor complicating matters is the pivotal role of uranium complexation. In both the hexavalent and pentavalent oxidation states, the uranyl cation is a linear molecule with five or six available coordination sites in the equatorial plane around the uranium atom.[6,7] In the tetravalent state, uranium localizes its electrons taking on octahedral or higher (7-, 8-, or 9-fold) coordination.[8,9] Uranyl is capable of forming strong complexes with oxyanions such as carbonate, filling coordination sites in the equatorial plane. Uranium groundwater speciation is dominated by uranium carbonate complexes when dissolved CO_2 is present.[10]

Carbonate has a significant effect on uranium chemistry in the environment by enhancing its solubility proportionally to carbonate concentration[11,12] and increasing it in systems where no significant hexavalent uranium is present.[13,14] Except in certain biologic mechanisms,[15] carbonate is known to inhibit uranium reduction to U(IV) completely.[16] Even under reducing conditions, uranium can incorporate itself into carbonates or ferric oxides as a hexavalent species.[17−20] From a thermodynamic standpoint, complexation of U(VI) by carbonate drives its reduction potential to significantly more negative values, eliminating a wide range of otherwise useful target reductant species. Complexation can further modify the ET behavior of a species by modifying the intrinsic electron affinity of a molecule, as well as possibly creating a steric hindrance that impedes the close approach of a reductant species. Hence, complexation with carbonate affects the driving force for ET as well as the mechanism, and therefore the rate of the reaction. It has been shown that the electrochemical behavior of the uranyl carbonate system is kinetically limited via electrode methods.[21] Those same electrochemical methods have been used to determine the redox potential of the U(VI)/U(V) couple in carbonate solutions: −0.820, −0.760, −0.778, and −0.3 versus SHE.[16,21−23]

Uranium reduction behavior is complicated by the fact that in many studies it has been observed to be influenced strongly by ET kinetics.[24,25] Homogeneous reduction of U(VI) by Fe(II) in aqueous solution was found to be slow even though partial reduction was predicted to be exothermic; instead it required the presence of solid phases to catalyze the reduction reaction.[26−28] Yet in most cases the intermediate oxidation state U(V) is short-lived, often consumed quickly by rapid ET in disproportionation reactions.[29] Very little information is available on the chemical conditions controlling uranium ET kinetics in general, due in large part to a limited number of reliable techniques for quantitatively identifying U(V).[16,21,30,31] Rates for the elementary U(VI)−U(V) self-exchange ET reaction are estimated to be slow.[32]

While the electronic structure of U(VI) is well understood in solid oxide phases, it is unclear how this structure transforms upon stepwise reduction. U(IV) is found to have little or no double-bonding character of the ligating bonds in solid-phase

† Stony Brook University.
‡ Pacific Northwest National Laboratory.

10.1021/jp062325t CCC: $33.50
Published on Web 07/19/2006

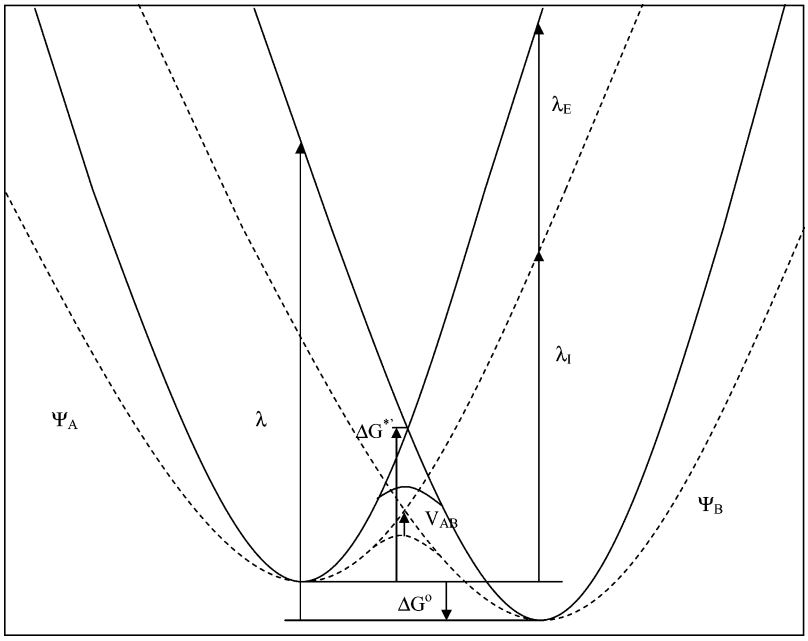

Figure 1. Diagram showing the specific application of Marcus theory to this system. Diabatic potential energy surfaces are shown as parabolic functions, separately for both the intrinsic (dashed line) and solvent (solid line) contributions. The thermodynamic free energy is shown as $\Delta G°$. Since the adiabatic curve does not account for solvent, we added the solvent component to estimate the total diabatic energy barrier, which is represented as the difference between the two horizontal lines in the crossing region.

oxides such as UO_2, and pathways to octahedral, or higher, coordination from the linear uranyl molecule as a result of stepwise reduction of U(VI) are unknown. As will be shown in this study, the later stages of this process may involve protonation of axial oxygen atoms during the conversion from U(V) to U(IV). However, we will show below for triscarbonato uranyl that this second ET step is thermodynamically uphill. Therefore the rate for the second ET step is not relevant here. Proton-coupled electron transfer (PCET) is an important aspect in the ET chemistry of many systems including, as will be demonstrated here, U(VI) to U(V) ET. As such, in part of this study we examine the role PCET mechanisms play in determining the ET rate. Although PCET is a very underdeveloped topic in geochemical systems, we note here that this aspect for the uranium system may demonstrate a possible tie between the ET behavior and solution conditions such as pH, a link that has been given very little previous attention in the uranium literature.[24,33]

In this study we present a detailed, theoretical analysis of the homogeneous ET behavior of uranyl carbonate in aqueous solution, specifically for the case where the reductant is Fe(II). The theoretical apparatus is based on Marcus' two-state ET model. The computational approaches involve the use of molecular dynamics (MD) simulations and Hartree−Fock (HF) and density functional theory (DFT) molecular orbital calculations. The focus is to compute the stepwise ET kinetics for the reduction of triscarbonato U(VI) by two Fe(II) atoms. MD simulations are used to model the interaction between aqueous Fe(II) and triscarbonato U(VI). Predictions for the structure and thermodynamic stability of the ensuing ET encounter complex are given. While no thermodynamic stability data for this particular complex are available to our knowledge, triscarbonato uranyl is known to form a strong complex with two Ca cations.[1,34] Therefore it is likely that the complex with two divalent iron cations is similarly stable. Here we will show this to be the case using MD simulations. Then we apply ab initio calculations to the computation of the two ET rates for stepwise intramolecular reduction of U(VI) by the two Fe(II) atoms. We compute the driving forces, reorganization energies, and electronic coupling matrix elements that enter into Marcus' ET model. This approach aims to determine a fundamental understanding of the kinetic behavior for uranium reduction by ferrous iron in the presence of carbonate.

Electron Transfer Model. The applied ET model is very similar to that reported by Rosso and co-workers[35−38] in several earlier studies involving Fe(II/III) ET. For additional details, the reader is referred to those studies and to standard texts and reviews of modern ET theory. Primary categories of reactions in the current system are encounter complex formation, ET, and PCET. Because the relevant initial oxidation states in the encounter complex are two Fe(II) atoms and one U(VI) atom, we will use II/II/VI to denote the initial electronic configuration Fe(II)/Fe(II)/U(VI), II/III/V for the intermediate configuration after the first ET step, and III/III/IV for the final configuration after the second ET step.

In all cases the iron atoms are treated as having a high-spin electronic configuration, such that Fe(II) is always in a $t_{2g}^4 e_g^2 d^6$ state and Fe(III) is always in a $t_{2g}^3 e_g^2 d^5$ state. The majority electron spins on the two iron atoms were taken as spin-parallel (ferromagnetic), with the minority spin on each iron atom comprising the donor electrons for the two ET reactions. Because these minority spin electrons each go into an empty U 5f orbital,[39−41] the total spin multiplicity is preserved through ET (spin multiplicity = 9); hence the ET reactions are "spin-allowed", which is a requirement in modern ET theory.[42]

For each ET step, within the encounter complex, we utilize the approach outlined by Marcus[43] based on two diabatic ET states ψ_A and ψ_B. The state ψ_A corresponds to the electronic state of the ET "reactants", and ψ_B corresponds to the electronic state of the ET "products" (Figure 1). Hence, for the first ET step, ψ_A is the II/II/VI state and ψ_B is the II/III/V state. For the second ET step ψ_A is the II/III/V state and ψ_B is the III/III/IV state.

ET is a Franck−Condon process, which means that ET is instantaneous relative to the rate of motion of nuclei. The potential energies of the three electronic states can be viewed

as having approximately quadratic dependence on nuclear coordinates in the encounter complex, which we will refer to as the internal coordinates, and in the surrounding solvent water, which we will refer to as the external coordinates. For any of the three electronic states, at equilibrium their energies correspond to minima in their respective potential energy surfaces. Thermally promoted fluctuations in the nuclear coordinates can lead to nuclear configurations for which the energies of states ψ_A and ψ_B are equal, the condition required for ET to occur. This coincidence condition corresponds to a crossing point between two potential energy surfaces (Figure 1).

The height of the barrier at the crossing point is the diabatic activation energy ($\Delta G^{*\prime}$) for ET. For potential energy surfaces that are similarly parabolic with respect to the nuclear coordinates, the diabatic activation energy is related in a simple fashion to the reorganization energy (λ) and the thermodynamic driving force for the ET step (ΔG°) as given by

$$\Delta G^{*\prime} = \frac{(\lambda + \Delta G^\circ)^2}{4\lambda} \tag{1}$$

The latter term, ΔG°, is the free energy difference between the energies of the reactants and products in their equilibrium nuclear configurations (Figure 1). The reorganization energy is the energy to distort the reactant's nuclear configuration into the product's nuclear configuration without having moved the electron (Figure 1). It is composed of two main contributions, one from distortion of bonds in the ET encounter complex, the internal part λ_I, and another from changing the polarization of the surrounding solvent, the external part λ_E.

Electronic interaction within the encounter complex between the donor and acceptor, such as that arising from superexchange interaction through bridging ligands, reduces the activation energy to ΔG^* (Figure 1). This effect is captured by the electronic coupling matrix element (V_{AB}), which is the interaction integral in a two-by-two configuration interaction problem for ψ_A and ψ_B at the crossing-point. V_{AB} effectively "smoothes" the intersection region, reducing $\Delta G^{*\prime}$ by the amount equal to V_{AB}, which gives the adiabatic barrier height ΔG^*.

In the following section, we outline our methods for the calculation of, among other things, the reorganization energy, the electronic coupling matrix element, and the driving force for each ET step.

Computational Methods

Molecular Dynamics Simulations. All of the MD simulations presented in this paper were performed with the computer code DL_POLY.[44] These calculations are based on the Born model of solids.[45] In this model, atoms are represented as point-charge particles that interact via long-range Coulombic forces and short-range interactions. The latter are described by parametrized functions and include a representation of the electron cloud repulsion, van der Waals attraction, and, where appropriate, many-body terms such as an angle-dependent term reproducing covalent effects in the carbonate anion.

Our model also accounts for the polarizability of anions by means of a mechanical shell model, which was first introduced by Dick and Overhauser.[46] In this model, a polarizable ion consists of two particles, a core and a shell, which are linked by a harmonic spring. All the simulations were performed in the NPT ensemble (constant number of particles, constant pressure, and constant temperature) and NVE ensemble (constant number of particles, constant volume, and constant energy) at 300 K and zero pressure. The Nosé-Hoover thermostat[47] and the Hoover barostat[47,48] kept temperature and pressure constant with parameters for a relaxation time of 0.5 ps. The Ewald summation method[49] was used to calculate electrostatic forces. An 8 Å cutoff was used for the short-range interactions, and the real part of the Ewald sum. The Verlet Leapfrog algorithm was used to integrate the equations of motion with a time step of 0.2 fs. The shells were given a mass of 0.2 au, their motion treated as that of the cores, following the adiabatic shell model first introduced by Mitchell and Fincham.[50]

The potential-based molecular dynamics approach relies upon the quality of the potential set employed; however, in most cases, we made use of previously tested potential parameters, and where this was not possible, new or modified potential parameters were validated against relevant experimental and theoretical data. The intra- and intermolecular interactions of water were described by the shell model of de Leeuw and Parker[51] with the modified hydrogen-bond potential of Kerisit and Parker.[52] The atomic charges and the potential parameters used to model the uranyl ion were taken from Guilbaud and Wipff.[53,54] In addition, we converted this model to a polarizable model by adding shells on the uranyl oxygens. The core−shell spring constant was that of Lewis and Catlow.[55] The potential parameters for the water−uranyl interactions were based on those of Guilbaud and Wipff.[53,54] The shell model version of the Guilbaud and Wipff uranyl model gives good agreement with theoretical and experimental characterizations of water coordination to the uranium ion in aqueous solution and the water cavity around uranyl oxygen ions as described by Hagberg et al.[56] (see Supporting Information). The atomic charges, core−shell spring constant, and potential parameters employed for the carbonate molecule were derived by Pavese et al.[57] and have been used many times successfully, principally to model calcium carbonate minerals[52,58−60] but also carbonate ions in aqueous solution.[61] This model has been used in combination with the de Leeuw and Parker water model on many occasions.[52,58,61]

The uranium−carbonate oxygen potential was taken to be the same as the uranium−water oxygen potential. Furthermore, a four-body potential was added to keep the six carbonate oxygens, which are directly coordinated to the uranium ion, in the same plane during an energy minimization of the gas-phase triscarbonato uranyl complex. Many times this was found to be the most stable configuration of the triscarbonato uranyl complex.[62−64] The predicted structures of the triscarbonato uranyl complex in the gas phase and in solution compare well with experimental and theoretical values (see Supporting Information). The potential parameters for the interactions between iron(II) and water were based on the iron−water potential of Curtiss et al.[65] and have been described previously.[66] This potential was modified to be compatible with the water model used in this work. Finally, the iron(II)−carbonate oxygen potential was based on the iron(II)−oxygen potential of Lewis and Catlow[55] and modified to give a good estimate of the lattice parameters of siderite ($FeCO_3$) and its bulk modulus (see Supporting Information). All the potential parameters used in this work are reported in Table 1 of the Supporting Information.

Quantum Mechanical Calculations. The MD simulations predicted the most stable structure and composition for the encounter complex in the II/II/VI electronic state. The predicted composition was $[Fe(II)Fe(II)U(VI)O_2(CO_3)_3(H_2O)_8]^0$. Two coordinating sites in the 6-fold coordination spheres of the two Fe atoms were occupied by carbonate oxygen atoms. The remaining Fe coordination sites were occupied by water oxygen atoms. The goal of the quantum mechanical calculations was to predict the minimum energy structures for this complex in

the II/II/VI, II/III/V, and III/III/IV electronic configurations at the DFT level of theory. We used the code NWChem[67] for these calculations. In each of the three electronic configurations, the total charge on the cluster is zero. We performed the energy minimizations on each cluster in the gas phase using the three-parameter hybrid HF/DFT exchange-correlation functional B3LYP.[68,69]

As mentioned previously, Fe(II) and Fe(III) atoms have high-spin d^6 and d^5 ground states, respectively.[70] UO_2^{2+} has a closed-shell singlet ground state with 12 valence electrons originating in the O 2p, and U 5f, 6d and 7s atomic orbitals.[39] UO_2^+ has a doublet ground state with the additional electron occupying a U 5f orbital. UO_2 has a triplet ground state in solid-phase UO_2 with two singly occupied U 5f orbitals. We optimized the II/II/VI, II/III/V, and III/III/IV configurations with a total spin multiplicity of 9, consistent with the transfer of iron atom minority spin electrons to open U 5f orbitals. The majority spins on the iron atoms have been assumed to align parallel.

We preoptimized the three structures at the B3LYP level using the 6-31G(d) basis set for H, C, O, and Fe and the LANL2DZ basis set for U for computational expediency. The preoptimized structures, and their wave functions, were used as the initial guess for final optimizations with a more robust basis set. The final basis set was as follows: 6-311++G(d,p) for H, O, and C, "Ahlrichs TZV" with Hay-Wadt diffuse and polarization functions for Fe, and the Stuttgart relativistic large-core basis set for U.[71−79] Total electronic energy differences from the final optimized structures were used to compute the values of $\Delta G°$ for the ET steps, assuming that these differences can be used to approximate the Gibbs free energy differences.

For each of the two ET steps, it is important to be able to predict the nuclear configuration at the curve crossing-points. To do this, we used the linear synchronous transit (LST) method to approximate the reaction coordinate. This approximation is reasonably accurate where relatively small nuclear displacements are involved,[80] as has been shown for the separate iron[36] and triscarbonato uranyl components of our system.[81] The LST method assumes that the ET reactant and product geometries can be linearly combined to produce intermediate structures, according to

$$X_n = \epsilon X_p + (1 - \epsilon)X_r \tag{2}$$

where X represents a set of nuclear coordinates for the reactants (r) and products (p) and their linear mixture (n), and ϵ is the mixing parameter that refers to the extent of progress along the reaction pathway. As was done for the equilibrium configurations, a spin multiplicity of 9 was used to compute the wave functions for the intermediate configurations by the LST method.

We used the quasi-diabatic method described by Farazdel et al.[80] to compute V_{AB}, as implemented in NWChem.[67] At the intersection, the splitting can be obtained by solving the secular equation

$$\begin{vmatrix} H_{AA} - E & H_{AB} - ES_{AB} \\ H_{AB} - ES_{AB} & H_{BB} - E \end{vmatrix} = 0 \tag{3}$$

where $H_{ij} = \langle\psi_i|H|\psi_j\rangle$ and i and j are equal to A or B, H is the total electronic Hamiltonian, $S_{AB} = \langle\psi_A|\psi_B\rangle$, and E is the energy eigenvalue. The two roots of the secular equation give the upper and lower adiabatic surfaces (Figure 1). The energy difference between the two adiabatic surfaces at the crossing point is computed as

$$2V_{AB} = (1 - S_{AB}^2)^{-1}[{}^1/_4(H_{AA} - H_{BB})^2 - (H_{AA} + H_{BB})H_{AB}S_{AB} + H_{AA}H_{BB}S_{AB}^2 + H_{AB}^2]^{1/2} \tag{4}$$

For computation of λ, we took advantage of the separability of the internal and external parts. The internal part was computed by the direct method described in Rosso et al.[35] This involves calculating the energy of the product' electronic state in the nuclear configuration of the reactant, the so-called charge-reversed (excited-state) condition. However, in the current case, the appropriate wave functions for the charge-reversed state could not be obtained; in practice, B3LYP seems to overestimate the delocalization of the electron, perhaps owing to the self-interaction error.[82−87] This made it difficult to obtain the pure product state in the reactant nuclear configuration, and vice versa. Attempts to obtain converged wave functions in the charge-reversed state often converged to the ground state instead. So to approximate the diabatic surfaces, we fit parabolas through the minima in the DFT potential energy surfaces and estimated diabatic crossing-points as $\Delta G^* + V_{AB}$, where ΔG^* is the adiabatic crossing-point barrier height computed by DFT. We used these fit surfaces to estimate λ_I (Figure 1).

The external reorganization energy (λ_E) was computed by use of Marcus' continuum expression, which gives[88]

$$\lambda_E = (\Delta e)^2(1/2r_1 + 1/2r_2 - 1/r)(1/d_{op} - 1/d_{stat}) \tag{5}$$

where r_1 and r_2 are radii for the donor and acceptor cavities, r is the distance between their centers, d_{op} is the optical dielectric constant (taken as 1.77 for water), and d_{stat} is the static dielectric constant (taken as 78.39 for water).[89] Values of r were taken from the final optimized structures. Cavity radii were chosen by averaging the computed lengths of M−O bonds. We took the average of the λ_E values for both products and reactants evaluated at the adiabatic crossing point (Figure 1).

Given the computed values of $\Delta G°$ (taken as $\sim\Delta E$), λ, and V_{AB} from the quantum mechanical calculations, first-order ET rate constants were computed from

$$k_{et} = \nu_n \exp[-((\Delta G° + \lambda)^2/4\lambda - V_{AB})/kT] \tag{6}$$

where ν_n is taken as a typical M−O stretching frequency, 10^{13} s^{-1}.[70] This equation assumes adiabatic behavior, which is justified given the computed values of V_{AB} we will present below. It also assumes nuclear tunneling effects are negligible, a reasonable assumption at ambient temperature.[90,91]

Results and Discussion

Encounter Complex Formation. We first equilibrated the triscarbonato uranyl complex in a cubic box containing 247 water molecules for 200 ps in the NPT ensemble. Then, an Fe(II) atom was introduced by replacing a water molecule in the vicinity of the triscarbonato uranyl complex and the system was equilibrated for 200 ps in the same conditions. We then carried out a series of independent molecular dynamics simulations in the microcanonical ensemble (NVE) to determine the potential of mean force of the Fe(II)−triscarbonato uranyl ion pair.

In each calculation, the distance between the centers of mass of the iron atom and triscarbonato uranyl complex was kept fixed. This means that we make the assumption that the reaction coordinate for the association process is the vector defined by the two centers of mass. As the triscarbonato uranyl complex can rotate with respect to the centers of mass vector, our choice of reaction coordinate is an approximation, which could result in the energy barriers being misrepresented slightly. However,

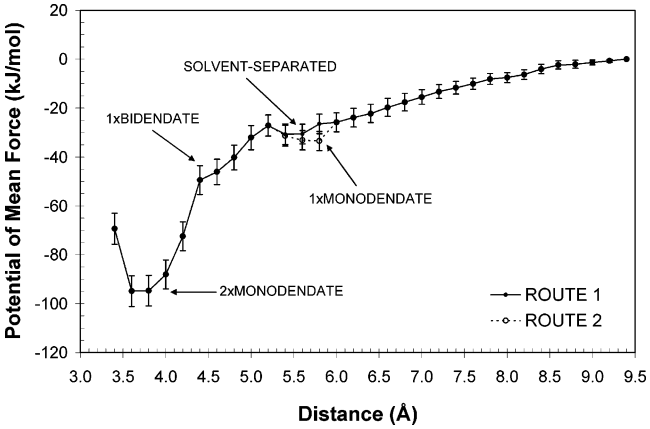

Figure 2. Potential of mean force of the Fe(II)−triscarbanato uranyl ion pair. Routes 1 and 2 represent two possible association mechanisms. "1×" and "2×" indicate how many carbonate groups are binding the iron atom in a monodentate or bidentate fashion. See text for a more detailed description of the labels and Supporting Information for figures of the complexes.

this approach is sufficient to identify the preferred association sites and compute the free energy change of the overall association process. This energy change is obtained by integrating the average force required to keep the two species at each set distance from the maximum separation to the point of interest.

A total of 30 calculations were performed to obtain points between 3.4 and 9.2 Å. In each calculation, the system is equilibrated for 2 ps and the average force is collected over 100 ps. The potential of mean force is shown in Figure 2. In the region between 9.2 and 8.6 Å, the hydration shells of the two species are complete, and there is some hydrogen bonding between the two shells. As the two species approach closer than 8.6 Å, a water molecule of the triscarbonato uranyl hydration shell is displaced and a water molecule from the iron hydration shell forms a hydrogen bond with a carbonate oxygen. As the two species draw nearer, a second hydrogen bond is formed from about 6.8 Å. A minimum in the free energy, shown as "solvent-separated" in Figure 2 (see Supporting Information for a figure of each complex mentioned in this section), is reached when a third hydrogen bond between a water molecule of the iron hexaaquo complex and a carbonate oxygen is formed at a distance of 5.5 Å. However, this minimum is shallow, and our calculations suggest that the residence time of iron in this site is likely to be short. From there, there is a small energy barrier (∼3 kJ/mol) for the hexaaquo iron complex to lose two water molecules and bind to a carbonate group in a bidentate fashion ("1×bidentate" in Figure 2). According to Figure 2, this is not a minimum in free energy but a short flattening of the curve. However, this might be due to our choice of the reaction coordinate. There is a strong driving force for the iron atom to then move to a position where it is coordinated to two oxygen atoms from two separate carbonate groups at a distance of about 3.6 Å, labeled "2×monodentate" in Figure 2. In addition, the large energy barrier for dissociation suggests that the iron residence time at this site is remarkably long. The free energy change of the overall process is calculated, from the potential of mean force at 3.6 Å, to be -95 ± 6 kJ/mol. The error bars in Figure 2 were estimated by calculating the standard deviation of the mean when the simulation was divided into five blocks. Furthermore, the overall interaction energy change can be computed from the difference in energy between the simulations at 9.2 and 3.6 Å and is found to be -157 ± 8 kJ/mol. Therefore, assuming that the interaction energy change is a good approximation for the enthalpy change, our calculations suggest a significant entropic contribution (about 60 kJ/mol) to the free energy change for complex formation.

There is a second possible route for the iron atom to attach at the 2×monodentate site. Rather than forming a third hydrogen bond, the hexaaquo iron complex can lose a water molecule to bind directly to a carbonate oxygen atom that is not coordinated to the uranium ion, "1×monodentate" in Figure 2. This minimum is relatively shallow too, and hence we expect this configuration of the complex to have a similar lifetime as that of the solvent-separated ion pair. The small difference in free energy between the two routes for distances shorter than 5.0 Å is due to uncertainties. To conclude, the potential of mean force clearly shows that the 2×monodentate site is the most energetically favored site and is kinetically stable.

To give some approximation of the lifetime of iron in the association sites mentioned above, we carried out two MD simulations whereby the iron atom was initially positioned either at the 1×monodentate or at the solvent-separated site. Both simulations were run for 200 ps. Figure 3 shows the distance between the iron atom and three of the carbonate oxygen atoms for the first 60 ps of each simulation. In the first simulation (Figure 3, top panel), the iron atom escaped from the 1×monodentate site after 20 ps to bind to a second oxygen of the same carbonate group. After residing in this site for another 15 ps, it then moved again to bind at the 2×monodentate site, where it stayed for the remaining of the simulation. In the second simulation (Figure 3, bottom panel), the iron atom first resided for about 15 ps at the solvent-separated site and then moved to the 1×bidentate site for 25 ps. Finally, it moved to the 2×monodentate site, where it stayed for the remaining of the simulation. Although we cannot compute precise average residence times from so few events, these calculations show that the residence time of iron in the solvent-separated, 1×monodentate, and 1×bidentate sites is short and on the order of a few tens of picoseconds. In summary, these calculations confirm the main conclusion drawn from the potential of mean force: the 2×monodentate site is clearly the most favorable association site, and iron and triscarbonato uranyl can form a very stable ternary complex.

Finally, we investigated the association of the iron triscarbonato uranyl complex with a second iron atom. We did not compute a second potential of mean force, as it was not expected to be significantly different. However, we calculated the energy change due to the second iron associating at the 2×monodentate site from three separate molecular dynamics calculations, namely, those of Fe(II), $[FeUO_2(CO_3)_3]^{2-}$, and $[Fe_2UO_2(CO_3)_3]$ in solution. The energy change is reduced to -119 ± 21 kJ/mol. Although the energy change has slightly decreased, it is still large and negative, which strongly suggests that the association of an additional iron atom will result in the formation of a stable species.

Equilibrium Structures and Energies. Given the predictions of the MD simulations, we were led to conclude that the 2×monodentate docking structure was most appropriate for each of the two Fe(II) atoms complexing the triscarbonato uranyl molecule. This gave the final encounter complex a composition of $[Fe_2UO_2(CO_3)_3(H_2O)_8]^0$. This cluster then became the focal point of our intramolecular ET kinetic calculations performed via DFT. The initial goals of the DFT calculations were to (1) find minimum energy structures for the II/II/VI, the II/III/V, and the III/III/IV electronic configurations; (2) determine the relative energies of these electronic configurations; and (3) from these relative energies, infer pathways for ET. Here we first

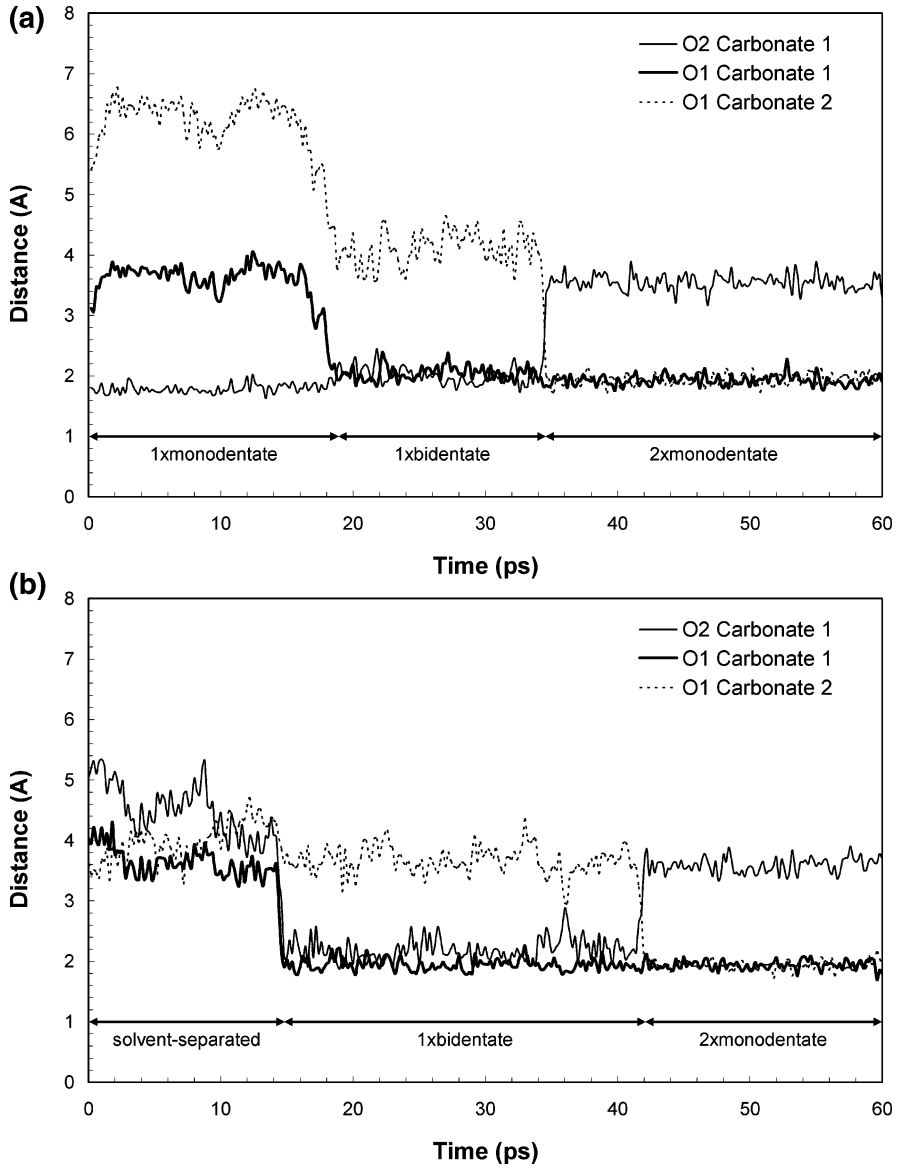

Figure 3. Graphs showing the distance between iron and three carbonate oxygens in two simulations of $[FeUO_2(CO_3)_3]^{-2}$ in solution: (top panel) the iron atom is initially placed at the 1 × monodentate site; (bottom panel) the iron is initially placed at the solvent-separated site.

discuss structural details of the optimized clusters in the II/II/VI, II/III/V, and III/III/IV electronic configurations.

Table 1 lists selected structural parameters for the II/II/VI, II/III/V, and III/III/IV electronic configurations optimized by DFT. The initial energy minimization was performed on the II/II/VI electronic configuration, starting from a nuclear configuration derived from the MD simulations. The iron atoms are bonded to two oxygens from two separate carbonates (2×monodentate), and the remaining four coordination sites on each of the two iron atoms are occupied by water molecules. The optimized geometry for the II/II/VI configuration consists of nearly the same bonding topology as suggested by the MD simulations, although the lack of hydrogen bonding to surrounding bulk water in quantum mechanical calculation leads to some subtle differences. The coordination of the uranium atom in the equatorial plane is 5-fold, consisting of two pairs of oxygen atoms from two carbonate ligands, and the fifth equatorial oxygen atom is from the third carbonate ligand (Figure 4). This third carbonate ligand bridges the two coordination spheres of the iron atoms. These aspects are the same in the MD and DFT predictions (see Supporting Information). However, in the DFT calculations, an oxygen atom on the third carbonate ligand is the acceptor site of a proton transfer (PT), transforming it into a bicarbonate ligand; the proton originates from a nearby water molecule attached to an iron atom during the energy minimization process (Figure 4). Also, the planarity of the equatorial carbonates is slightly broken in the DFT calculation. Both the intramolecular proton transfer and the decrease in the planarity of the carbonate ring may arise from the gas-phase treatment in the DFT calculation. It is possible that inclusion of a polarizable continuum model (PCM) to describe the remaining absent solvent would have changed the propensity for the proton transfer to occur. However, we expect it to be of little consequence to the computed ET rate parameters such as the reorganization energies and electronic coupling matrix elements in this system due to the peripheral nature of the proton transfer. Use of a PCM model was also found to be computationally unwieldy.

Starting from the II/II/VI optimized structure, energy minimization of the II/III/V electronic configuration yields a structure that differs in four main respects (the initial asymmetry, specifically the OH ligand, determined which iron would oxidize

TABLE 1: Calculated Metal−Oxygen Distances and ET (Fe−U) Distances

from Fe1 to		from Fe2 to		from U to	
atom	distance (Å)	atom	distance (Å)	atom	distance (Å)
		II/II/VI Configuration			
O_{H2O}	2.344	O_{H2O}	2.302	O_{UO}	1.780
O_{H2O}	2.220	O_{H2O}	2.113	O_{UO}	1.775
O_{H2O}	2.163	O_{H2O}	2.200	O_{CO}	2.454
O_{OH}	1.950	O_{H2O}	2.277	O_{CO}	2.362
O_{CO}	2.761	O_{CO}	2.090	O_{CO}	2.352
O_{CO}	2.010	O_{CO}	2.018	O_{CO}	2.434
				O_{CO}	2.493
avg	2.241	avg	2.167	avg	2.236
U	3.864	U	4.065		
		II/III/V Configuration			
O_{H2O}	2.218	O_{H2O}	2.287	O_{UO}	1.827
O_{H2O}	2.118	O_{H2O}	2.234	O_{UO}	1.826
O_{OH}	1.896	O_{H2O}	2.189	O_{CO}	2.486
O_{OH}	1.896	O_{H2O}	2.231	O_{CO}	2.422
O_{CO}	2.026	O_{CO}	2.070	O_{CO}	2.776
O_{CO}	2.233	O_{CO}	1.980	O_{CO}	2.557
				O_{CO}	2.622
avg	2.065	avg	2.165	avg	2.359
U	3.856	U	3.973		
		II/III/V_{int} Configuration			
O_{H2O}	2.224	O_{H2O}	2.239	O_{UO}	1.833
O_{H2O}	2.117	O_{H2O}	2.185	O_{UO}	1.827
O_{H2O}	2.109	O_{H2O}	2.270	O_{CO}	2.486
O_{OH}	1.896	O_{H2O}	2.184	O_{CO}	2.440
O_{CO}	1.923	O_{CO}	2.132	O_{CO}	2.518
O_{CO}	2.061	O_{CO}	1.970	O_{CO}	2.530
				O_{CO}	2.968
avg	2.055	avg	2.202	avg	2.372
U	3.747	U	4.047		
		III/III/IV Configuration			
O_{OH}	1.879	O_{H2O}	2.417	O_{UOH}	2.077
O_{OH}	1.878	O_{H2O}	2.209	O_{UOH}	2.098
O_{OH}	1.928	O_{H2O}	2.105	O_{CO}	2.437
O_{H2O}	2.342	O_{OH}	1.843	O_{CO}	2.522
O_{CO}	2.046	O_{CO}	2.001	O_{CO}	2.454
O_{CO}	3.283	O_{CO}	1.922	O_{CO}	2.537
				O_{CO}	2.537
avg	2.226	avg	2.083	avg	2.380
U	4.073	U	3.991		

when the electronic configuration was changed). First, one of the five equatorial U−OCO_2 bonds extends by 0.43 Å to 2.78 Å (Table 1), effectively reducing the number of equatorial oxygen atoms to four, accompanied by slight adjustment of the other two carbonate ligand positions. Second, the average Fe−O bond distance decreases for the oxidized iron atom, as expected from the smaller ionic radius of Fe(III) relative to Fe(II). Third, the average U−O distance increases in accordance with the change in the oxidation state of the uranium atom from U(VI) to U(V). And fourth, a proton from a water ligand on the Fe(III) atom transfers to an oxygen atom on a carbonate ligand that bridges the Fe(III) atom to the U(V) atom (Figure 5). This is the second water molecule to undergo dissociation in the same iron solvation shell, in agreement with the tendency of Fe(III) to hydrolyze more readily than Fe(II).[70] Hence, the comparison of the minimum energy structures for the II/II/VI and II/III/V configurations suggests that the first ET step is accompanied by an intramolecular PT that takes place between a water molecule of the first solvation shell of an iron atom and the carbonate ring.

For the III/III/IV configuration, two main features were found in this optimized structure. First, two protons, one from water ligands of each iron atom, transfer to the axial oxygen atoms of the central uranium cation (Figure 6). A second observation

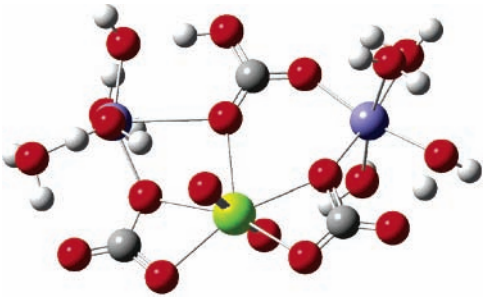

Figure 4. Diagram of the computed minimum energy structure for the II/II/VI electronic configuration, showing the protonated bridging bicarbonate. The yellow sphere is the uranium atom, red spheres are oxygen atoms, blue spheres are iron atoms, gray spheres are carbon atoms, and white spheres are hydrogen atoms.

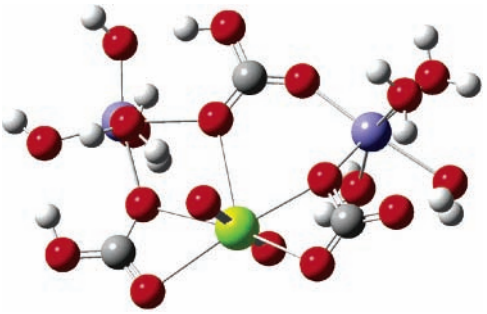

Figure 5. Diagram of the computed equilibrium structure for the II/III/V electronic configuration. See Figure 4 caption for atom legend. The monodentate carbonate bond is extended. The protonated carbonate in the upper right is transferred during the II/II/VI → II/III/V ET.

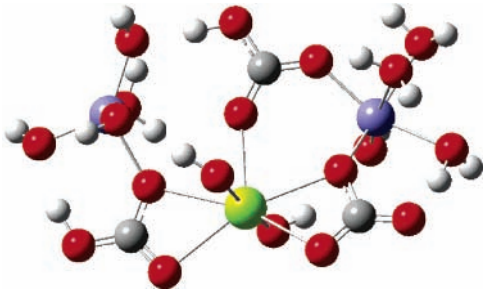

Figure 6. Diagram showing the computed minimum energy structure of the III/III/IV electronic configuration. See Figure 4 caption for atom legend. Protons have transferred to the axial oxygen atoms on the uranium cation.

regarding this structure is that the coordination on one of the Fe atoms is reduced from six to five. This is a result of recoordination of the third carbonate with the uranium; it might not have occurred if additional explicit waters of solvation were present.

In their minimum energy nuclear configurations, the computed energy difference for the first ET step (II/II/VI → II/III/V) is −30.4 kJ/mol, and for the second step (II/ III/V → III/III/IV) it is +13.9 kJ/mol at the DFT level of theory. Assuming that the total electronic energy differences are reasonable estimates for the free energy differences, the calculations suggest that the III/III/IV configuration is energetically unfavorable relative to the II/III/V configuration, and therefore the III/III/IV configuration will not be an end product of ET in this system. In other words, we find that the II/III/V is the most stable electronic configuration in this ternary complex. This

result is consistent with the well-established finding from experiment that the stability of U(V) is substantially enhanced by carbonate complexation of the uranyl cation.[15,21,22] Therefore, with respect to the reduction rate of U(VI) in this complex, the ET rate of primary importance is the first step, which is accompanied by a single PT.

Electron-Transfer Pathways. To predict the kinetics of the first ET step, we need to compute the height of the ET barrier. This requires that we have an accurate nuclear configuration for the transition state. In the past we have had success using the LST approach to approximate the transition-state structure for ET,[92−94] and we apply this approach here. However, in this case, the DFT calculations just described suggest two possible pathways for the II/II/VI → II/III/V conversion. The first is a sequential ET/PT pathway, where ET is followed by PT or vice versa. The second is a concerted ET/PT, where the transfers occur simultaneously. Both pathways fall under the general category of PCET. In his recent review on this topic, Mayer[95] outlines the distinction between the two pathways as arising from whether a reaction intermediate must be invoked; that is, an intermediate structure or reaction between the ET and PT. Concerted PCET is considered as not requiring an intermediate but also does not require that the ET and PT occur simultaneously. Here we evaluate the barriers for both the sequential and concerted PCET pathways for the II/II/VI → II/III/V step, where again the ET is the transfer of an electron from the Fe(II) atom to the U(VI) atom and the PT is the transfer of a proton from a first-shell water molecule to a carbonate ligand. We define the sequential pathway (hereafter $PCET_{seq}$) as the ET step followed by the PT step, with the ordering arising from the finding that the ET should be slower than the PT in this case and therefore is more likely to be rate-limiting for the sequence. We define the concerted pathway (hereafter $PCET_{con}$) as the ET and the PT occurring simultaneously.

By application of the LST approach to the optimized structures of the II/II/VI and II/III/V configurations, the potential energy surfaces for both PCET pathways can be estimated. Given the values computed for the electronic coupling matrix element, discussed below, we find that both PCET pathways fall within the adiabatic regime. Thus the potential energy surface on which the PCET reaction evolves is the adiabatic surface (Figure 7). For the $PCET_{con}$, the barrier maximum is located at an energy of 109.6 kJ/mol above the equilibrium energy of the II/II/VI configuration and at a mixing parameter value of ∼0.4 on the reaction coordinate (Figure 7, top panel). Thus the $PCET_{con}$ is characterized by an adiabatic barrier height of +109.6 kJ/mol (relative to the potential energy of the reactants) and a driving force of −30.4 kJ/mol.

For the $PCET_{seq}$ pathway, we require an additional energy-minimized structure, which is the one in the II/III/V electronic configuration except without the accompanying PT. To achieve this, we ran an energy minimization equivalent to the others starting from the optimized structure for the II/II/VI electronic configuration, except with the O−H distances fixed. We refer to this configuration as $II/III/V_{int}$, where int indicates intermediate. Selected structural details for this energy minimized structure are listed in Table 1. In its equilibrium nuclear configuration, the energy of $II/III/V_{int}$ was found to lie +6.9 kJ/mol higher in energy than the equilibrium energy for the II/II/VI configuration. Therefore, this is the energetic location for the intermediate in the $PCET_{seq}$ pathway. Application of the LST method to the ET step and separately to the PT step yields barrier heights of +51.0 kJ/mol relative to the II/II/VI configuration (for the ET step), and +24.2 kJ/mol relative to the $II/III/V_{int}$ configuration (for the PT step). Thus the adiabatic potential energy surface for the $PCET_{seq}$ pathway is composed of two barriers (Figure 7, bottom panel), with the barrier for the ET step approximately twice as large as the barrier for the PT step.

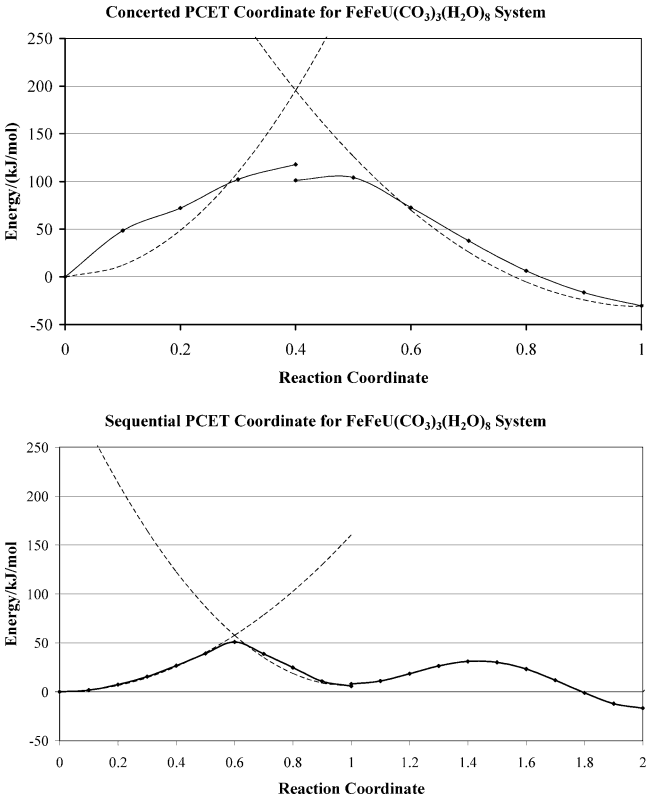

Figure 7. Adiabatic (solid) and diabatic (dashed) potential energy surfaces for the concerted (top panel) and sequential (bottom panel) proton-coupled electron-transfer pathways. The adiabatic curves were computed at the DFT level of theory with a reaction coordinate based on the LST method. The reaction coordinate scales from 0 to 1 for the $PCET_{con}$ pathway. For the $PCET_{seq}$ pathway, the reaction coordinate scales from 0 to 1 for the ET step and 1 to 2 for the PT step. The diabatic curves were approximated as parabolas passing through the sum of the adiabatic barrier height plus the calculated values of the electronic coupling matrix elements.

Electronic Coupling. The electronic coupling at the crossing points for both the concerted and sequential PCETs is of interest for determining whether the ET components of these reactions fall under the adiabatic or nonadiabatic (also called diabatic) regimes. For the nonadiabatic regime, passage through the crossing point does not necessarily lead to the ET products being formed, with the transition probability depending on the square of V_{AB}. For the adiabatic regime, the system evolves on an adiabatic potential energy surface resembling a double-well potential and the transition probability at the crossing point is treated as 100%, independent of V_{AB}. Using the methods outlined above, we compute V_{AB} values using HF wave functions at the crossing-point geometries derived by DFT. We do this because the DFT treatment leads to partial electron delocalization near the crossing-point regions, as is self-evident in the potential energy surfaces shown in Figure 7, and therefore the diabatic states are not accessible in the DFT approach. For the crossing point in $PCET_{con}$, we compute $V_{AB} = 85.8$ kJ/mol, and for the crossing point in $PCET_{seq}$, we compute $V_{AB} = 6.8$ kJ/mol. Both values are above the typical room-temperature adiabaticity criterion of 2.4 kJ/mol,[96] which means that both forms of PCET can be treated as adiabatic.

Reorganization Energy. The above analysis indicates that both forms of PCET for the II/II/VI → II/III/V ET process are adiabatic. Therefore the ET rate can be determined directly from the potential energy surfaces simply by knowing the barrier height. However, because of the methodological approach taken, this would ignore the possibility that the external reorganization energy could be significant relative to the internal reorganization energy and thereby modify the barrier height. Therefore it is of interest to evaluate both λ_I and λ_E, quantities related to the diabatic potential energy surfaces, to estimate the magnitude of this effect. As described in the Computational Methods section, we approximated the diabatic potential energy surfaces by fitting quadratic functions to energetic minima and diabatic barriers estimated as the adiabatic barrier height plus V_{AB} (Figure 7). This allowed an estimate of λ_I, to which we added the value for λ_E computed from Marcus' continuum equation.

Values of λ_I computed from the DFT potential energy surfaces in combination with the computed values of V_{AB} are 242.5 kJ/mol (sequential) and 924.1 kJ/mol (concerted). The reorganization energy of the solvent λ_E was calculated to be 144.3 kJ/mol. The total values of λ then becomes 386.8 and 1068.3 kJ/mol, respectively. The contribution of the solvent to the reorganization energy, and therefore the barrier height, is clearly significant.

Overall Rates of Reaction

The calculated rate for the $PCET_{con}$ pathway is extremely slow, at $\sim 7 \times 10^{-17}$ s^{-1}, which is effectively zero. The calculated rates for the two steps within the $PCET_{seq}$ pathway are 6×10^{-1} s^{-1} for the ET step and 9×10^{8} s^{-1} for the subsequent PT step. Hence, the $PCET_{seq}$ pathway is predicted to be overwhelmingly the faster of the two pathways, and therefore sequential PCET is the predicted mechanism. Given the sequential nature of the two elementary steps involved, the slower of the two rates is limiting. Thus we expect that the conversion of hexavalent uranium to pentavalent uranium in the current system occurs only at a rate of about 1 s^{-1}. Clearly the sequential pathway is also the chemically intuitive choice in this case, because the proton that transfers moves from a water ligand to a carbonate ligand, neither of which coincides with the electron donor and acceptor sites. Concerted PCET is more likely to involve ET and PT with similar donor and acceptor locations.[95]

The question of overall reduction rate (k) is important in light of the need to obtain values that can be compared directly with experiment. However, no experimental reduction rates for this system are yet available to our knowledge. A chemist's first instinct might be to apply an equilibrium approximation for the formation of the encounter complex and assume steady state as follows: $k = K_{eq}k_{et}[Fe]^2[U]$. However, given the −249 kJ/mol driving force predicted for the formation of the encounter complex, this approach is not appropriate. A more appropriate model[97] would assume that 100% of the available Fe and triscarbonato uranyl would form complexes, resulting in the following expression: $k = k_{et}[M]$, where [M] is the metal with a lower concentration.

Collectively, our analysis leads to the conclusion that the dominant final oxidation state of uranium in this system is pentavalent. Given that it is already well-known that carbonate complexation tends to stabilize pentavalent uranium,[16,22,81,98] our calculations are consistent with this observation. Given that the II/III/V → III/III/IV ET process was predicted to be strongly endergonic and that this step apparently is coupled with protonation of the two axial oxygen atoms (complicating the use of the computational approach taken here), we are unable at this time to assess the potential for production of U(IV) and subsequent solid phases in this system. From our analysis, this ET system should steadily progress toward and stabilize primarily pentavalent uranium.

In summary, this study finds that Fe(II) should form stable ternary complexes with triscarbonato U(VI) in aqueous solution and that within these complexes uranium should be reduced principally to the pentavalent uranium oxidation state. Two ferrous iron atoms are predicted to bind to the three-membered carbonate ring of the uranium−carbonate complex. ET from one of the iron atoms to the central uranium atom is thermodynamically favorable and should occur adiabatically by sequential ET coupled with a proton transfer, with a slow overall rate of ~ 1 s^{-1}. The subsequent reduction of U(V) to U(IV) has a significant thermodynamic barrier. This latter step also appears to be coupled with the protonation of the axial oxygen atoms, as a possible precursor to the transformation of the uranyl moiety toward 7-fold coordinated U(IV). Thus, a major finding of this study is that pentavalent uranium is predicted to be stabilized in this system, likely on time scales that are amenable for experimental study.

Acknowledgment. M.C.F.W. and M.A.A.S. are grateful for financial support from NSF−Chemistry through the Center for Environmental Molecular Science at Stony Brook, Award CHE-0221934, and a supplement that allowed M.C.F.W. to take up residence at the Environmental Molecular Sciences Laboratory (EMSL) at Pacific Northwest National Laboratory (PNNL) to conduct part of this work. The EMSL is funded by the U.S. Department of Energy (DOE) Office of Biological and Environmental Research (OBER). K.M.R. and S.K. acknowledge support from the Stanford Environmental Molecular Sciences Institute, jointly funded by NSF−Chemistry and the DOE-OBER. PNNL is operated by Battelle for the DOE under Contract DE-AC06-76RLO 1830.

Supporting Information Available: Table of the potential parameters; tables comparing the structural parameters of the uranyl ion in aqueous solution, the triscarbonato uranyl complex (both MD and DFT), and siderite mineral obtained in this work with published experimental and theoretical data; figures of the four iron triscarbonato uranyl complexes shown in Figure 2; and table showing a comparison of the distances calculated from the potential model and DFT calculations for the II/II/VI iron triscarbonato uranyl complex. This material is available free of charge via the Internet at http://pubs.acs.org.

References and Notes

(1) Guillaumont, R.; Fanghänel, T.; Fuger, J.; Grenthe, I.; Neck, V.; Palmer, D. A.; Rand, M. H. *Update on the Chemical Thermodynamics of Uranium, Neptunium, Plutonium, Americium and Technetium*; Elsevier: Amsterdam, 2003.

(2) Gonzalez-Gil, G.; Amonette, J. E.; Romine, M. F.; Gorby, Y. A.; Geesey, G. G. *Geochim. Cosmochim. Acta* **2005**, *69*, 1145.

(3) Sani, R. K.; Peyton, B. M.; Amonette, J. E.; Geesey, G. G. *Geochim. Cosmochim. Acta* **2004**, *68*, 2639.

(4) Liu, C.; Zachara, J.; Zhong, L.; Kukkadupa, R.; Szecsody, J.; Kennedy, D. *Environ. Sci. Technol.* **2005**, *39*, 4125.

(5) Qafoku, N. P.; Zachara, J. M.; Liu, C. X.; Gassman, P. L.; Qafoku, O. S.; Smith, S. C. *Environ. Sci. Technol.* **2005**, *39*, 3157.

(6) Neck, V.; Kim, J. I. *Radiochim. Acta* **2000**, *88*, 815.

(7) Mizuoka, K.; Grenthe, I.; Ikeda, Y. *Inorg. Chem.* **2005**, *44*, 4472.

(8) Rybakov, V. B.; Ansalov, L. A.; Kolesnichenko, V. L.; Kulikovskii, B. N.; Volkov, S. V. *Russ. J. Coord. Chem.* **2000**, *26*, 594.

(9) Grenthe, I.; Wanner, H.; Forest, I. *Chemical thermodynamics of uranium*; Elsevier: New York, Amsterdam, 1992.

(10) Eelless, M. P.; Lee, S. Y. *Water, Air, Soil Pollut.* **1998**, *107*, 147−162.

(11) Echevarria, G.; Sheppard, M. I.; Morel, J.; Aviramt, A. *J. Environ. Radioact.* **2001**, *53*, 257.
(12) Abdelouas, A.; Lutze, W.; Nuttall, E. *J. Contam. Hydrol.* **1998**, *34*, 343−361.
(13) Gu, B. H.; Wu, W.-M.; Vogel, M. A. G.; Yan, H.; Fields, M. W.; Zhou, J. Z.; Fendorf, S.; Criddle, C.; Jardine, P. M. *Environ. Sci. Technol* **2005**, *39*, 4841.
(14) Iwatsuki, T.; Arthur, R.; Ota, K.; Metcalfe, R. *Radiochim. Acta* **2004**, *92*, 789.
(15) Gu, B. H.; Wu, W.-M.; Ginder-Vogel, M. A.; Yan, H.; Fields, M. W.; Zhou, J. Z.; Fendorf, S.; Criddle, C.; Jardine, P. M. *Environ. Sci. Technol.* **2005**, *39*, 4841.
(16) Mizuguchi, K.; Park, Y.-Y.; Tomiyasu, H. *J. Nucl. Sci. Technol.* **1993**, *30*, 542.
(17) Duff, M. C.; Coughlin, J. U.; Hunter, D. B. *Geochim. Cosmochim. Acta* **2002**, *66*, 3533−3547.
(18) Fuller, C. C.; Bargar, J. R.; Davis, J. A.; Piana, M. J. *Environ. Sci. Technol.* **2002**, *36*, 158.
(19) Mason, C. F. V.; Turney, W. R. J. R.; Thomson, B. M.; Lu, N.; Longmire, P. A.; Brause, C. J. C. *Environ. Sci. Technol.* **1997**, *31*, 2707.
(20) Qiu, S. R.; Lai, H.-F.; Roberson, M. J.; Hunt, M. L.; Amrhein, C.; Giancarlo, L. C.; Flynn, G. W.; Yarmoff, J. A. *Langmuir* **2000**, *16*, 2230.
(21) Morris, D. E. *Inorg. Chem.* **2002**, *41*, 3542.
(22) Caja, J.; Pravdic, V. *Croat. Chem. Acta* **1969**, *41*, 213.
(23) Capdeleva, H.; Vitorge, P. *J. Radioanal. Nucl. Chem.* **1990**, *143*, 403.
(24) Newton, M. D. *J. Phys. Chem.* **1975**, *79*, 2795.
(25) Nash, K. L.; Sullivan, J. C. *Kinetics and Mechanisms of Actinide Redox and Complexation Reactions*; Sykes, A. G., Ed.; Academic Press: New York, 1986; Vol. 5, p 185.
(26) Liger, E.; Charlet, L.; Van Cappellen, P. Surface catalysis of uranium(VI) reduction by iron(II)—Spectroscopic evidence for sorption and reduction. *Geochim. Cosmochim. acta* **1999**, *63*, 2939.
(27) Ilton, E. S.; Haiduc, A.; Cahill, C. L.; Felmy, A. R. *Inorg. Chem.* **2005**, *44*, 2986.
(28) Privalov, T.; Schimmelpfennig, B.; Wahlgren, U.; Grenthe, I. *J. Phys. Chem. A* **2003**, *107*, 587.
(29) Newton, T.; Baker, F. *Inorg. Chem.* **1965**, *4*, 1166.
(30) Mizuoka, K.; Ikeda, Y. *Radiochim. Acta* **2004**, *92*, 631.
(31) Mizuoka, K.; Tsushima, S.; Hasegawa, M.; Hoshi, T.; Ikeda, Y. *Inorg. Chem.* **2005**, *44*, 6211.
(32) Valiela, I.; Costa, J.; Foreman, K.; Teal, J. M.; Howes, B.; Aubrey, D. *Biogeochemistry* **1990**, *10*, 177.
(33) Newton, T. W. *The Kinetics of the Oxidation−Reduction Reactions of Uranium, Neptunium, Plutonium and Americium in Aqueous Solutions*; Oak Ridge, Tennessee, Technical Information Center, Office of Public Affairs, U.S. Energy Research and Development Administration: Springfield, Virginia, 1975; Vol. TID-26506.
(34) Bernhard, G.; Geipel, G.; Reich, T.; Brendler, V.; Amayri, S.; Nitsche, H. *Radiochim. Acta* **2001**, *89*, 511.
(35) Rosso, K. M.; Smith, D. M. A.; Dupuis, M. *J. Chem. Phys.* **2003**, *118*, 6455.
(36) Rosso, K. M.; Rustad, J. R. *J. Phys. Chem. A* **2000**, *104*, 6718.
(37) Rosso, K. M.; Morgan, J. J. *Geochim.Cosmochim. Acta* **2002**, *66*, 4223.
(38) Iordanova, N.; Dupuis, M.; Rosso, K. M. *J. Chem. Phys.* **2005**, *122*, 144305.
(39) Kaltsoyannis, N. *Chem. Soc. Rev.* **2003**, *32*, 9.
(40) Kaltsoyannis, N. *J. Chem. Soc., Dalton Trans.* **1997**, 1.
(41) Kaltsoyannis, N. *Inorg. Chem.* **2000**, *39*, 6009.
(42) Polihronov, J. G.; Hedstrom, M.; Hummel, R. E.; Cheng, H.-P. *J. Luminesc.* **2002**, *96*, 119.
(43) Marcus, R. A. *Annu. Rev.* **1964**, 155.
(44) Smith, W.; Forester, T. R. *J. Mol. Graphics* **1996**, *14*, 136.
(45) Born, M.; Huang, K. *Dynamical Theory of Crystal Lattices*; Oxford University Press: Oxford, U.K., 1954.
(46) Dick, B. G.; Overhauser, A. W. *Phys. Rev.* **1958**, *112*, 90.
(47) Hoover, W. G. *Phys. Rev. A* **1985**, *31*, 1695.
(48) Melchionna, S.; Ciccotti, G.; Holian, B. L. *Mol. Phys.* **1993**, *78*, 533.
(49) Ewald, P. P. *Ann. Phys.* **1921**, *64*, 253.
(50) Mitchell, P. J.; Fincham, D. *J. Phys.: Condensed Matter* **1993**, *5*, 1031.
(51) de Leeuw, N. H.; Parker, S. C. *Phys. Rev. B* **1998**, *58*, 13901.
(52) Kerisit, S.; Parker, S. C. *J. Am. Chem. Soc.* **2004**, *126*, 10152.
(53) Guilbaud, P.; Wipff, G. *J. Phys. Chem.* **1993**, *97*, 5685.
(54) Guilbaud, P.; Wipff, G. *J. Mol. Struct.* **1996**, *366*, 55.
(55) Lewis, G. V.; Catlow, C. R. A. *J. Phys. C: Solid State Phys.* **1985**, *18*, 1149.
(56) Hagberg, D.; Karlstrom, G.; Roos, B. O.; Gagliardi, L. *J. Am. Chem. Soc.* **2005**, *127*, 14250.
(57) Pavese, A.; Catti, M.; Parker, S. C.; Wall, A. *Phys. Chem. Miner.* **1996**, *23*, 89.
(58) de Leeuw, N. H.; Parker, S. C. *J. Phys. Chem. B* **1998**, *102*, 2914.
(59) Duffy, D. M.; Harding, J. H. *J. Mater. Chem.* **2002**, *12*, 3419.
(60) Kristensen, R.; Stipp, S. L. S.; Refson, K. *J. Chem. Phys.* **2004**, *121*, 8511.
(61) Kerisit, S.; Cooke, D. J.; Spagnoli, D.; Parker, S. C. *J. Mater. Chem.* **2005**, *15*, 1454.
(62) Hemmingsen, L.; Amara, P.; Ansoborlo, E.; Field, M. J. *J. Phys. Chem. A* **2000**, *104*, 4095.
(63) Gagliardi, L.; Grenthe, I.; Roos, B. O. *Inorg. Chem.* **2001**, *40*, 2976.
(64) Vazquez, J.; Bo, C.; Poblet, J. M.; de Pablo, J.; Bruno, J. *Inorg. Chem.* **2003**, *42*, 6136.
(65) Curtiss, L. A.; Halley, J. W.; Hautman, J.; Rahman, A. *J. Chem. Phys.* **1987**, *86*, 2319.
(66) Kerisit, S.; Rosso, K. M. *Geochim. Cosmochim. Acta* **2006**, *70*, 1888.
(67) Aprà, E.; Windus, T. L.; Straatsma, T. P.; Bylaska, E. J.; de Jong, W.; Hirata, S.; Valiev, M.; Hackler, M.; Pollack, L.; Kowalski, K.; Harrison, R.; Dupuis, M.; Smith, D. M. A.; Nieplocha, J.; V., T.; Krishnan, M.; Auer, A. A.; Brown, E.; Cisneros, G.; Fann, G.; Fruchtl, H.; Garza, J.; Hirao, K.; Kendall, R.; Nichols, J.; Tsemekhman, K.; Wolinski, K.; Anchell, J.; Bernholdt, D.; Borowski, P.; Clark, T.; Clerc, D.; Dachsel, H.; Deegan, M.; Dyall, K.; Elwood, D.; Glendening, E.; Gutowski, M.; Hess, A.; Jaffe, J.; Johnson, B.; Ju, J.; Kobayashi, R.; Kutteh, R.; Lin, Z.; Littlefield, R.; Long, X.; Meng, B.; Nakajima, T.; Niu, S.; Rosing, M.; Sandrone, G.; Stave, M.; Taylor, H.; Thomas, G.; van Lenthe, J.; Wong, A.; Zhang, Z. *NWChem, A Computational Chemistry Package for Parallel Computers*, Version 4.7; Pacific Northwest National Laboratory: Richland, WA, 2005.
(68) Stevens, P. J.; Devlin, F. J.; Chabalowski, C. F.; Frisch, M. J. *J. Phys. Chem.* **1994**, *98*, 11623.
(69) Becke, A. D. *J. Chem. Phys.* **1993**, *98*, 5648.
(70) Richens, D. T. *The Chemistry of Aqua Ions; Synthesis, Structure and reactivity; A periodic tour through the elements*; John Wiley: Chichester, U.K., 1997.
(71) Hariharan, P. C.; Pople, J. A. *Theor. Chim. Acta* **1973**, *28*, 213.
(72) Francl, M. M.; Pietro, W. J.; Hehre, W. J.; Binkley, J. S.; Gordon, M. S.; DeFrees, D. J.; Pople, J. A. *J. Chem. Phys.* **1982**, *77*, 3654.
(73) Rassolov, V.; Pople, J. A.; Ratner, M.; Windus, T. L. *J. Chem. Phys.* **1998**, *109*, 1223.
(74) Krishnan, R.; Binkley, J. S.; Seeger, R.; Pople, J. A. *J. Chem. Phys.* **1980**, *72*, 650.
(75) Clark, T.; Chandrasekhar, J.; Spitznagel, G. W.; Schleyer, P. V. R. *J. Comput. Chem.* **1983**, *4*, 294.
(76) Ortiz, J. V.; Hay, P. J.; Martin, R. L. *J. Am. Chem. Soc.* **1992**, *114*, 2736.
(77) Schafer, A.; Huber, C.; Ahlrichs, R. *J. Chem. Phys.* **1994**, *100*, 5829.
(78) http://www.emsl.pnl.gov/forms/basisform.html.
(79) Frisch, M. J.; Trucks, G. W.; Schlegel, H. B.; Scuseria, G. E.; Robb, M. A.; Cheeseman, J. R.; Montgomery, J. A., Jr.; Vreven, T.; Kudin, K. N.; Burant, J. C.; Millam, J. M.; Iyengar, S. S.; Tomasi, J.; Barone, V.; Mennucci, B.; Cossi, M.; Scalmani, G.; Rega, N.; Petersson, G. A.; Nakatsuji, H.; Hada, M.; Ehara, M.; Toyota, K.; Fukuda, R.; Hasegawa, J.; Ishida, M.; Nakajima, T.; Honda, Y.; Kitao, O.; Nakai, H.; Klene, M.; Li, X.; Knox, J. E.; Hratchian, H. P.; Cross, J. B.; Adamo, C.; Jaramillo, J.; Gomperts, R.; Stratmann, R. E.; Yazyev, O.; Austin, A. J.; Cammi, R.; Pomelli, C.; Ochterski, J. W.; Ayala, P. Y.; Morokuma, K.; Voth, G. A.; Salvador, P.; Dannenberg, J. J.; Zakrzewski, V. G.; Dapprich, S.; Daniels, A. D.; Strain, M. C.; Farkas, O.; Malick, D. K.; Rabuck, A. D.; Raghavachari, K.; Foresman, J. B.; Ortiz, J. V.; Cui, Q.; Baboul, A. G.; Clifford, S.; Cioslowski, J.; Stefanov, B. B.; Liu, G.; Liashenko, A.; Piskorz, P.; Komaromi, I.; Martin, R. L.; Fox, D. J.; Keith, T.; Al-Laham, M. A.; Peng, C. Y.; Nanayakkara, A.; Challacombe, M.; Gill, P. M. W.; Johnson, B.; Chen, W.; Wong, M. W.; Gonzalez, C.; Pople, J. A. *Gaussian 03W*, revision C.2; Gaussian, Inc.: Wallingford, CT, 2004.
(80) Farazdel, A.; Dupuis, M.; Clementi, E.; Aviramt, A. *J. Am. Chem. Soc.* **1990**, *112*, 4206.
(81) Docrat, T. I.; Mosselmans, J. F. W.; Charnock, J. M.; Whiteley, M. W.; Collison, D.; Livens, F. R.; Jones, C.; Edmiston, M. J. *Inorg. Chem.* **1999**, *38*, 1879.
(82) Cora, F.; Stachiotti, M. G.; Catlow, C. *J. Phys. Chem.* **1997**, *101*, 3945.
(83) Lundberg, M.; Siegbahn, P. E. M. *J. Chem. Phys.* **2005**, *122*, Art. No. 224103.
(84) Baric, D.; Maksic, Z. B. *J. Phys. Chem. A* **2003**, *107*, 11577.
(85) Polo, V.; Kraka, E.; Cremer, D. *Mol. Phys.* **2002**, *100*, 1771.
(86) Polo, V.; Kraka, E.; Cremer, D. *Theor. Chem. Acc.* **2002**, *107*, 291.
(87) Csonka, G. I.; Johnson, B. G. *Theor. Chem. Acc.* **1998**, *99*, 158.
(88) Marcus, R. A. *J. Chem. Phys.* **1956**, *24*, 966.
(89) Marcus, R. A.; Sutin, N. *Biochim. Biophys. Acta* **1985**, *811*, 265.
(90) Skodje, R. T.; Truhlar, D. G.; Garrett, B. C. *J. Chem. Phys.* **1982**, *77*, 5955.

(91) Skodje, R. T.; Truhlar, D. G. *J. Phys. Chem.* **1981**, *85*, 624.
(92) Peng, C. Y.; Schlegel, H. B. *Isr. J. Chem.* **1993**, *33*, 449.
(93) Jensen, A. *Theor. Chim. Acta* **1983**, *63*, 269.
(94) Halgren, T. A.; Lipscomb, W. N. *Chem. Phys. Lett.* **1977**, *49*, 225.
(95) Mayer, J. M. *Annu. Rev. Phys. Chem.* **2004**, *55*, 363.
(96) Gratzel, M. *Heterogeneous photochemical electron transfer*; CRC Press: Boca Raton, FL, 1989.
(97) Moraes, J. E.; Quina, F. H.; Nascimento, C. A.; Silva, D. N.; Chiavone-Filho, O. *Environ. Sci. Technol.* **2004**, *38*, 1183.
(98) Wester, D. W.; Sullivan, J. C. *Inorg. Chem.* **1980**, *19*, 2838.